New Journal of Physics
The open access journal for physics

Different views on the electronic structure of nanoscale graphene: aromatic molecule versus quantum dot

M Wießner[1,2], N S Rodríguez Lastra[1,2], J Ziroff[1,2], F Forster[1,2], P Puschnig[3], L Dössel[4], K Müllen[4], A Schöll[1,2,5] and F Reinert[1,2]

[1] Universität Würzburg, Experimentelle Physik VII and Röntgen Research Center for Complex Material Systems (RCCM), D-97074 Würzburg, Germany
[2] Karlsruher Institut für Technologie (KIT), Gemeinschaftslabor für Nanoanalytik, D-76021 Karlsruhe, Germany
[3] Institute of Physics, Karl-Franzens-Universität Graz, Graz, Austria
[4] Max-Planck-Institut für Polymerforschung, D-55021 Mainz, Germany
E-mail: Achim.schoell@physik.uni-wuerzburg.de

New Journal of Physics **14** (2012) 113008 (12pp)
Received 23 January 2012
Published 7 November 2012
Online at http://www.njp.org/
doi:10.1088/1367-2630/14/11/113008

Abstract. Graphene's peculiar electronic band structure makes it of interest for new electronic and spintronic approaches. However, potential applications suffer from quantization effects when the spatial extension reaches the nanoscale. We show by photoelectron spectroscopy on nanoscaled model systems (disc-shaped, planar polyacenes) that the two-dimensional band structure is transformed into discrete states which follow the momentum dependence of the graphene Bloch states. Based on a simple model of quantum wells, we show how the band structure of graphene emerges from localized states, and we compare this result with *ab initio* calculations which describe the orbital structure.

[5] Author to whom any correspondence should be addressed.

Contents

1. Introduction

Owing to its extraordinary properties and fascinating possible applications, graphene is currently one of the most interesting materials in physics and material sciences [1]. In this respect, small planar carbon-based molecules have also attracted considerable interest since they represent a well-defined starting point for the preparation of larger and more complex graphene-like systems. In particular, two-dimensional polyacenes, i.e. planar π-conjugated molecules consisting of small sub-units resembling the honeycomb lattice of graphite, are promising candidates for such a controlled bottom-up approach [2–5]. Among these, coronene ($C_{24}H_{12}$) and hexa-*peri*-hexabenzocoronene (HBC, $C_{42}H_{18}$) (see figure 1(a) for molecular structures) are comparatively large and at the same time thermally stable compounds, consisting of 6 and 12 edge-fused benzene rings, respectively. Thus, the central carbon ring experiences the same chemical environment as in graphene (see figure 1(a)). When deposited on the noble metal surfaces Ag(111) or Au(111), coronene and HBC form notably ordered monolayer phases. All molecules are oriented in the same way, so that the macroscopic angular resolved photoemission signal of the organic layer can be approximated by the signal of one individual molecule [6–8]. Although the films show a very high long-range order, as demonstrated by the electron diffraction measurements in figure 1(c), the structure differs obviously from that of graphene since the terminating hydrogen atoms separate the molecules laterally. This separation seems to suppress emergent lattice effects. This raises the question of whether the isolated molecule picture or the isolated quantum dot interpretation should be deployed in order to understand the electronic structure of graphene nanoarchitectures.

In this paper, we present angle-resolved photoelectron spectroscopy (ARPES) measurements of coronene and HBC on Ag(111) and compare these measurements with density functional theory (DFT) calculations of the molecular orbital structure of coronene and HBC and show how well the simplified quantum well model of graphene [9–15] describes the molecular electronic states.

2. Experimental and computational details

All experiments were performed in an ultrahigh vacuum system with a base pressure below 10^{-10} mbar. The coronene films were prepared in an attached preparation chamber by organic molecular beam deposition with a deposition rate of 0.05 ML min^{-1} onto clean and well-ordered Ag(111) single-crystal surfaces [16] at room temperature. The monolayer film quality

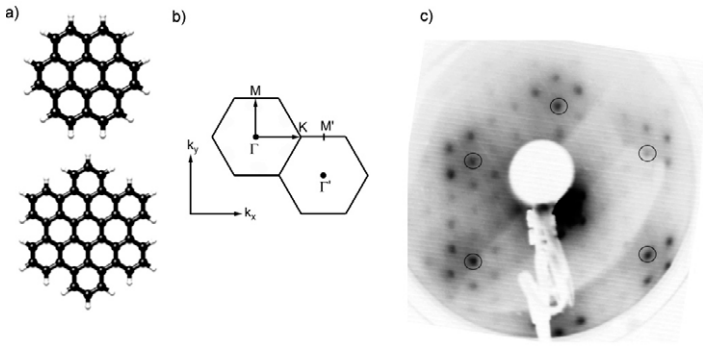

Figure 1. (a) Molecular structure of coronene (top) and HBC (bottom). (b) Two-dimensional Brillouin zone scheme of coronene on Ag(111). The high-symmetry points are shown, and primed characters mark the second Brillouin zone. (c) LEED image of $\approx$1 ML coronene on Ag(111) recorded at $E_{\mathrm{kin}} = 76\,\mathrm{eV}$ showing the 4×4 superstructure. The positions of substrate LEED spots are marked by black circles.

and thickness were characterized by monitoring the evolution of sharp spots of the low-energy electron diffraction (LEED) pattern in figure 1(c), i.e. the typical commensurate 4×4 superstructure of the first monolayer [7]. In contrast to multi-domain systems like in [17, 18], the present one-domain system provides the prerequisites for ARPES measurements, because the photoemission signal is not a sum of different rotational domains.

The photoemission measurements for coronene were obtained with a monochromatized vacuum ultraviolet lamp for He II_α radiation ($h\nu = 40.8\,\mathrm{eV}$) and a high-resolution photoelectron analyzer (Scienta R4000), leading to an overall energy resolution of about $\Delta E = 5\,\mathrm{meV}$. For measuring the angular-dependent photoelectron intensity, we used the angular mode of the analyzer, allowing the simultaneous detection of an emission window of $\theta = \pm 15^\circ$ in one direction, with a resolution of $\Delta\theta = 0.3^\circ$. To have access to a larger k-space region we tilted the sample additionally with a step width of 2°, providing an overall momentum resolution of approximately $\Delta k = 0.1\,\mathrm{\AA}^{-1}$ [19]. The equipotential plots ($I(E_B = \mathrm{const}, k_x, k_y)$) were integrated over an energy window of $\Delta E_B = 200\,\mathrm{meV}$, covering the main fraction of the photoemission line of the respective molecular orbital. The ARPES data show repeating intensity distributions after rotating the sample by 60°, so the six-fold symmetry of the system was used to generate the complete maps from the individual angle scans accordingly. The sample temperature during ARPES and LEED measurements was kept constant at about 70 K. The sample was checked repeatedly for possible beam damage or other deterioration effects. The photoemission measurements for HBC were obtained with a Scienta SES 200 high-resolution photoelectron analyzer, leading to an overall energy resolution of about $\Delta E = 10\,\mathrm{meV}$. The window for parallel detection in the angular mode was $\theta = \pm 7^\circ$ with a resolution of $\Delta\theta = 0.3^\circ$. To reduce beam damage, these measurements were carried out at a temperature of $T = 200\,\mathrm{K}$.

All DFT calculations were performed with the VASP code [20], which uses plane waves as basis functions and employs the projector augmented wave approach to account for treating core electrons [21]. Exchange and correlation effects are treated by using a generalized gradient approximation [22]. Since the plane wave basis set implies periodic boundary conditions,

calculations for isolated molecules are performed by using a supercell approach with a sufficient amount of vacuum in order to prevent wave function overlap across periodic replica of molecules. Thus, a coronene molecule is put into a box of size $20 \times 20 \times 12$ Å, HBC in a box of $24 \times 24 \times 12$ Å, and circum-coronene in a box of $26 \times 26 \times 12$ Å. For simulating photoemission intensity maps, either in the $k_x - k_y$ mode or in the energy distribution curve (EDC) mode $E_b - k$, we calculate the photoemission intensity with the one-step model and approximate the final state by a plane wave [23]. In order to obtain smooth momentum representations of the simulated photoemission intensity maps, we use a $6 \times 6 \times 3$ k-point sampling of the supercell's Brillouin zone. This numerical trick simply enhances the resolution of the simulated maps in reciprocal space. For the comparison with the graphene band structure, we used a free-standing layer of graphene in a repeated slab approach with a vacuum size of 20 Å and a k-point sampling of $18 \times 18 \times 1$. Note that we aligned the calculated HOMO of coronene and HBC with its measured binding energy and stretched all coronene, HBC and graphene energies by a factor of 1.1 to facilitate comparison with experiment. It is a well-known fact that DFT calculations employing the local density approximation (LDA) or the generalized gradient approximation (GGA) for the exchange-correlation functional not only severely underestimate band gaps of semi-conductors but also yield too small π-band widths of many systems including graphene—and hence also graphene-like molecules—which can be corrected by self-energy calculations within the so-called GW-approximation [24]. Moreover, in the presence of a metal, apart from a rigid energy shift of the DFT band structures of the isolated graphene/molecules, an additional renormalization of the energy axis may also occur [25].

3. The electronic structure of coronene and hexa-*peri*-hexabenzocoronene (HBC)

Figures 2(c) and (f) show angle integrated photoemission spectra, i.e. EDCs, of 1 ML coronene and HBC on Ag(111). For both samples we identify several peaks that we attribute to molecular signals. Three of these are labeled MO1, MO2, MO3 and are discussed in detail below. For coronene, the highest occupied molecular orbital (MO1) appears at $E_B = 2.5$ eV, whereas the HOMO of HBC lies at $E_B = 2.3$ eV. The next state follows at $E_B = 3.7$ eV for coronene (MO2), whereas for HBC additional intensity appears already at $E_B = 2.7$ eV, which can be attributed to the larger size of HBC compared to coronene. The most intense signal between $E_B = 3.8$ and 7.7 eV is due to the emission from the 4d states of the Ag substrate. Within this regime, no clear distinction between the photoemission intensity from the substrate and from the molecules is possible. More information can be gained when analyzing angle-resolved PES data as displayed in a color-scale plot in figures 2(b) and (e) for coronene and HBC, respectively. Here, the k-dependence of the PES intensity clearly makes the Ag sp-bands visible, which disperse between the Fermi edge and the 4d states at about 1 Å^{-1} and which are thus forming a nearly constant background in the angle-integrated EDCs. As in other organic monolayer systems [26–28], the Shockley state of Ag(111) [29] does not appear in the photoemission data, because it has most likely shifted above the Fermi level. Apart from these substrate features, we observe a strong and characteristic k-dependence of the molecular signals as seen in figures 2(b) and (e). The highest occupied molecular state (HOMO, labeled MO1), appears in both cases most intense near the $\overline{K}$-point at $k_x = 1.7$ Å^{-1}. The MO2 for coronene as well as the MO3 for HBC are a little closer to the Γ-point, whereas the coronene MO3 is a superposition of mainly two states, one exactly at Γ and one at $k_x = 2$ Å^{-1}.

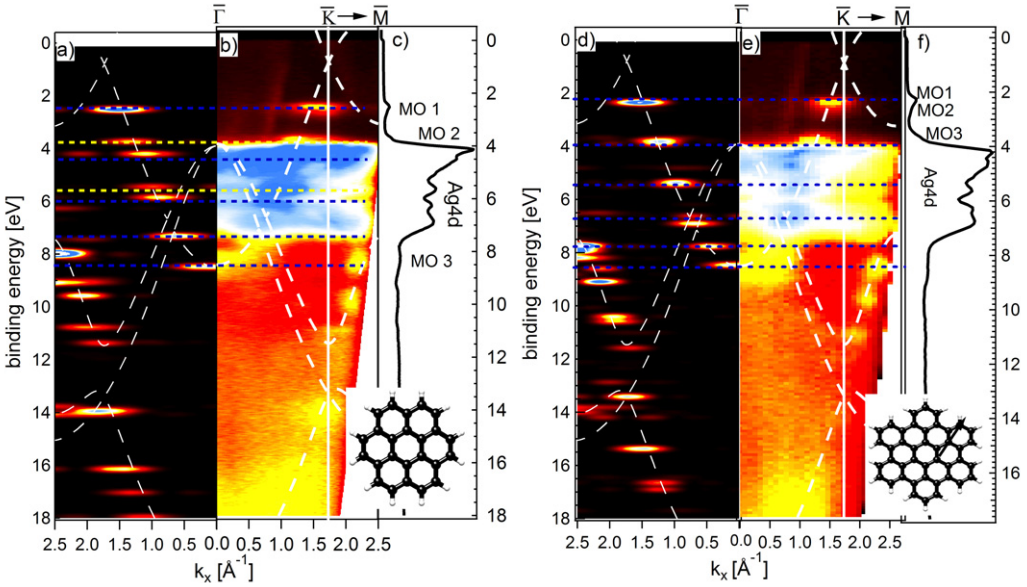

Figure 2. Photoemission intensity versus binding energy and parallel electron momentum in $\overline{\Gamma}-\overline{K}-\overline{M}$ direction for coronene (a)–(c) and HBC (d)–(f) showing in (a) and (d) the DFT calculated intensity for an isolated molecule and in (b) and (e) experimental data for 1 ML coronene or HBC, respectively, on Ag(111) with HeII_{α} radiation at $T = 70$ K. The white dashed lines in (b) and (e) represent the calculated band structure of graphene. Panels (c) and (f) display the EDC, after k-integration of the data in (b) and (e). The blue horizontal lines in (a), (b) and (d), (e) indicate the eigenvalues for graphene π-band electrons confined in a cylindrical quantum well, the yellow horizontal lines in (a), (b) mark some split-off states for coronene.

4. Coronene and HBC as π-conjugated molecules

This characteristic angular dependence of the photoemission intensity can be explained by starting from an *ab initio* description of the free molecule. As demonstrated for other systems [19, 23, 25, 30], a Fourier transformation of the molecular orbitals, describes the angular distribution of the photoemission intensity for planar compounds very well under certain preconditions [23]. This can be seen for the high-symmetry direction $\overline{\Gamma}-\overline{K}-\overline{M}$ in figures 2(a) and (d), where the series of discrete energy levels has clear intensity maxima in certain k_x-directions. These intensity patterns provide additional information if the full k_x–k_y-dependent intensity distribution for every single state is plotted.

Beginning with coronene, figure 3 compares the experimental results (figures 3(a)–(c)) with the corresponding calculated data (figures 3(d)–(f)). The orbitals closest to the Fermi level, in particular MO1, show a six-fold symmetry with maxima in the direction of the $\overline{K}$-points located at the corners of the dashed hexagon, similar to the Fermi surface of graphene [31]. The states MO2 and MO3 at higher binding energies have different intensity distributions. For MO2 the maxima are in the direction of $\overline{M}$. The slight shift of the maxima to lower k-values might be caused by the superposition of the molecular intensities with the underlying d-band emission of the substrate. The intensity distribution of MO3 is a superposition of

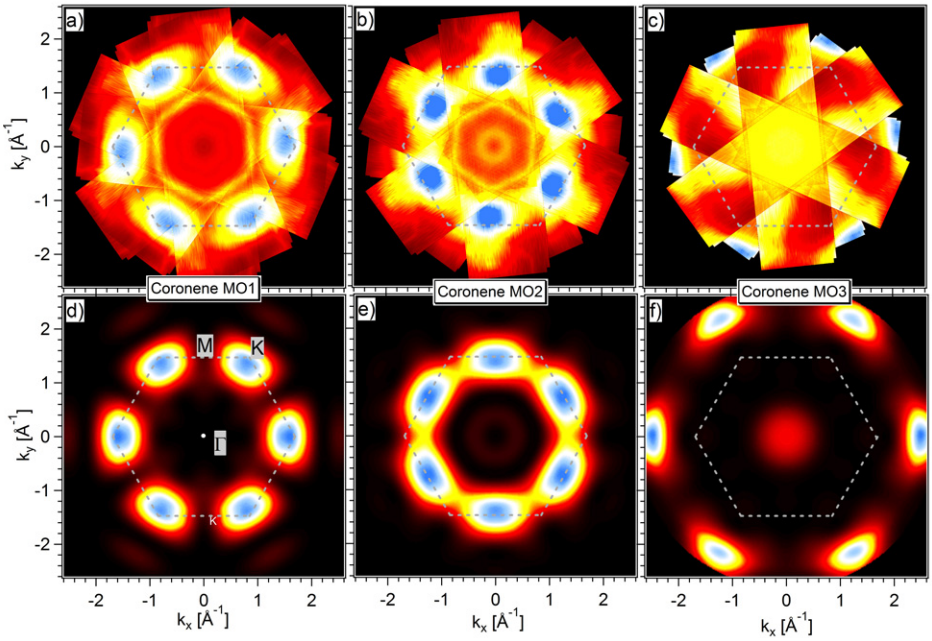

Figure 3. Experimental $k_{x,y}$-dependent ARPES intensity of the (a) MO1, (b) MO2 and (c) MO3 of coronene on Ag(111) measured with HeII$_\alpha$. Panels (d)–(f) show the corresponding DFT calculations for the isolated molecule at the respective photoelectron energies. The dotted hexagons represent the first Brillouin zone of graphene.

two different contributions, one with six-fold symmetry with maxima in the $\overline{K}$-direction and another one peaked at the $\overline{\Gamma}$-point, i.e. in the normal emission. These two contributions can also be distinguished in figure 2(b), where an intensity maximum appears at $E_B = 8.4$ eV near $k_\parallel = 0$ Å^{-1} (Γ-point) and another one at $k_\parallel \approx 2.0$ Å^{-1} (i.e. close to $\overline{M}$). The contributing real space wave functions differ. The intensity maximum near the Γ-point is given by the lowest coronene π-orbital, whereas the intensity at $k_\parallel \approx 2.0$ Å^{-1} is due to an orbital with σ-character. Note that the intensity of these states is much lower compared to the π-states, so that we could make them unambiguously visible in ARPES for the first time [25, 30, 32–34]. In the calculation these two orbitals are split in binding energy by 0.5 eV, which is due to self-interaction errors in π- and σ-orbitals. This results in an overestimation of the σ-orbital energy in our DFT-GGA calculations. In experiment, however, these two π- and σ-states show the same binding energy within the experimental energy resolution. Focusing on the experimental maps in figure 3, one has to consider the contributions from the substrate: in panels (a) (MO1) and (b) (MO2) the Ag sp-band emission appears as a hexagon around $k_\parallel \approx 1$ Å^{-1}. Additionally, the photoemission intensity in panel (b) contains some contribution from the adjacent Ag 4d-bands, which creates a broad background. Taking these results into account, the intensity distributions for MO1 and MO2 match the DFT calculations for the isolated molecule well, thus justifying our neglect of lattice effects for the organic overlayer. Note that for MO3 in panel (c) the signal-to-background ratio is lower than for MO1 or MO2 and the intensity maxima at higher k-values are not fully accessible with He II$_\alpha$-radiation. Despite these restraints we can predict the experimental intensity distribution from the DFT calculations.

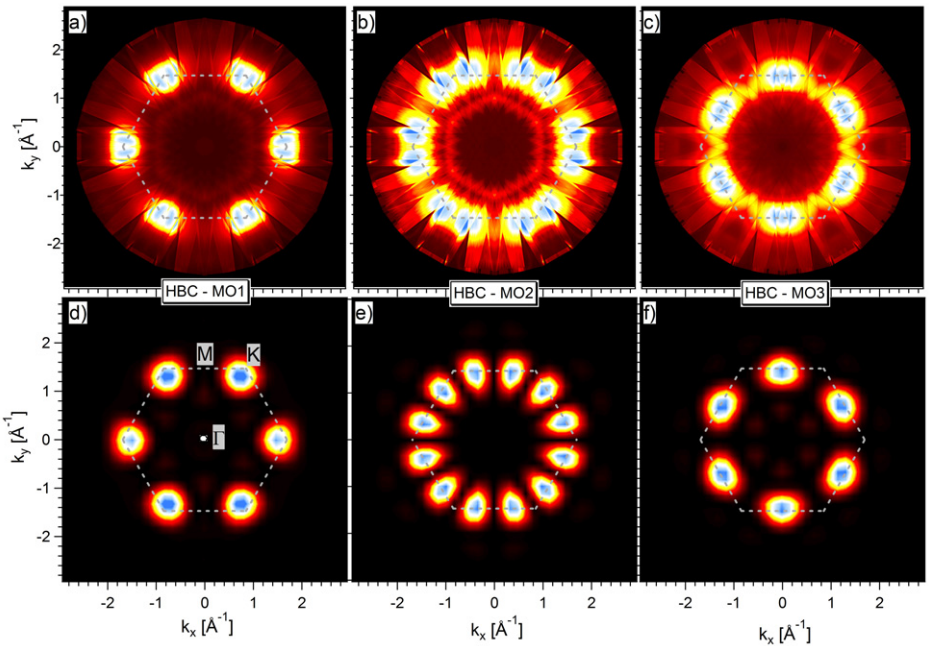

Figure 4. Experimental $k_{x,y}$-dependent ARPES intensity of the (a) MO1, (b) MO2 and (c) MO3 of HBC on Ag(111) measured with HeII$_\alpha$. Panels (d)–(f) show the corresponding DFT calculations for the isolated molecule at the respective photoelectron energies. The dotted hexagons represent the first Brillouin zone of graphene.

If we compare the equivalent findings for HBC in figure 4 with coronene in figure 3, we find that MO1 and MO3 of HBC are similar to MO1 and MO2 of coronene. The most obvious difference between these two states of coronene and HBC is the width in both the k_x- and k_y-directions. For HBC the MOs are sharper in k-space, due to the larger extent of the respective real-space wave function for HBC compared to coronene. In contrast MO2 of HBC is different. This orbital arises in the gap between two coronene states and is purely located at the outer six benzene rings of the HBC molecule. Due to the energetic proximity to MO1, we had to disentangle these two signals in the experimental data by a fit with two Gaussians. Again experiment and theory match nicely. The difference for MO2 might originate either from intensity from MO1 or from a slight distortion of the geometric structure of HBC on the silver substrate. Due to the stronger localization at the outer rings this orbital is expected to be very sensitive to such a distortion.

5. Graphene quantum wells

Alternatively, the electronic states of coronene and HBC can be described in a quantum well approach. Along this line, the electronic structure of the molecules can be understood as a local confinement of the electronic structure of an infinity graphene sheet. To illustrate this we have superposed the graphene valence bands as white dashed lines in figure 2 [35]. The first intriguing aspect is that all the molecular eigenstates appear along the graphene bands. This demonstrates that already the presence of the small graphene subunits of 2.5 Å size in

the coronene/HBC molecules anticipates properties of the infinite, two-dimensional graphene lattice [13–15, 36]. Therefore, the individual molecule can be regarded as graphene quantum wells, separated laterally by the hydrogen atoms. Since for finite systems, k is not an exact quantum number, the electronic states are broadened in k. The broadening in k is immediately connected to the finite number of periods of the real space wave function. This can be tested when comparing the linewidth in the k_x-direction of coronene with the larger HBC. As expected the linewidth decreases (about 7%) when increasing the size of the molecule. We can drive this approach one step further and approximate the disc-shaped HBC by a cylindrical potential with infinitely high potential wells. In such a case, the eigenvalues are given by the following expression [37]:

$$E_n = \frac{\hbar^2}{2m_{\text{eff}}r^2}\left[a_{m,n}\right]^2.$$

Here, $m_{\text{eff}} = 1.3m_{\text{e}}$ denotes the effective mass of the graphene π-band in a parabolic approximation around $\overline{\Gamma}$, and r is the radius of the cylindrical well which we approximate by half of the largest extent of the molecule, i.e. $r = 5.9$ Å for HBC. Finally, $a_{m,n}$ denotes the nth zeros of the mth Bessel function $a_{m,n}$. We have included the energy eigenvalues of the cylindrical well in the HBC ARPES data in figures 2(d) and (e) as horizontal dashed blue lines. They correspond to the lowest six energy levels for $n = 1$, where the energy of the lowest quantum well state was shifted to match the lowest π-state of HBC. The crossing points of the eigenenergy lines with the graphene π-band give a good approximation for the positions of MO1 and MO3 in energy and $k_{\|}$ and also match two high-intensity areas within the Ag 4d states. We would like to stress that this simple model for the cylindrical quantum well uses only two parameters, the effective mass of the π-band and the radius of the molecule, but neglects any substrate, lattice or many-body interactions. Thus, the good agreement between theory and experiment is impressive. For the other states at higher binding energies, this simple model cannot be applied, since the effective mass of the respective graphene bands changes with k_x. Note that for the smaller coronene molecule, the quantum well solutions do not fit as good as for HBC. This is reasonable since for the smaller coronene the approximation of infinite barrier height and cylindrical shape is obviously less valid than for HBC. For coronene the radius of the quantum well that provides a reasonable match to the experimental data is 5.0 Å, compared to the half of the extent of the molecule of 3.8 Å . Additionally, one has to include split-off states with the same energetic spacing (illustrated by the yellow lines in figures 2(a) and (b)) due to a lift of degeneracy due to the lower symmetry of the coronene compared to the quantum well.

To prove that the match for HBC and coronene is not accidental, we compare the DFT results of the even larger molecule circum-coronene with the quantum well solutions in the right panel of figure 5. Unfortunately, the experimental data are not straightforwardly accessible since this compound cannot be prepared by vacuum sublimation. One can clearly see that the main states in the DFT calculation can be described by the quantum well model, whereas a few additional and weaker states appear due to the lift of the degeneracy by changing from the cylindrical symmetry C_∞ of the quantum well model to the hexagonal symmetry C_6 of the molecule.

Figure 5 concludes our findings for the investigated disc-shaped molecules. The electronic structure of the molecules (figure 5 right) can be approximated by taking the π-band of graphene (figure 5 left) and applying a confining potential of the dimension of the molecule (figure 5 middle). The resulting solutions can predict the molecular states in both, energy and

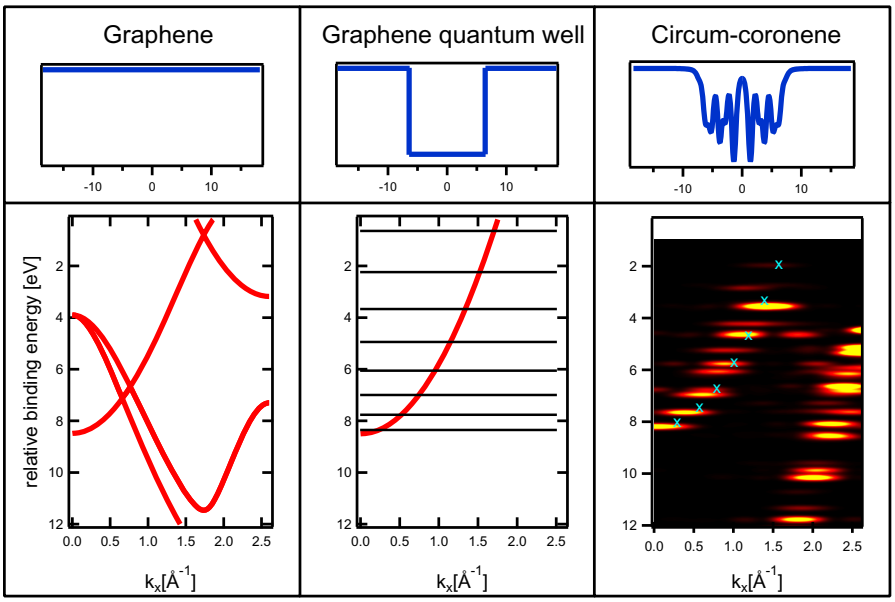

Figure 5. The relationship of graphene and circum-coronene. The top part shows in each case the radially averaged confining potential, which is absent in the free graphene layer. For the graphene quantum well in the middle, we use a cylindrical box and for the circum-coronene the potential is given by the molecular structure. The bottom shows in each case the respective calculated electronic structure in the $\overline{\Gamma}-\overline{K}-\overline{M}'$ direction. For the quantum well, the parabolic approximation of the π-band is plotted as the red curve, the solutions for the quantum well with a size of $r = 6.55$ Å are plotted as horizontal black lines. Their crossing points are superposed to the circum-coronene as cyan crosses. The additional states in the circum-coronene are related to the hexagonal symmetry of the system, which is omitted in the quantum well picture.

momentum position, although some additional split-off states appear. As for coronene, these arise due to the hexagonal symmetry of the molecule, which is omitted in the cylindrical quantum well model. Such a formation of lateral quantum well states is well known for other low-dimensional systems. On vicinal metal surfaces [38–40], periodically arranged step edges lead to a quantum well state formation of the Shockley state. Quantum confinement of surface-state-related wave functions also occurs between supramolecular chains in grating-like assemblies [41], in small metal islands [42] or in metal-organic networks [43]. Moreover, a few reports exist on organic molecular systems which show one-dimensional quasi-band structures, e.g. sexiphenyl, pentacene or alkane chain systems [30, 32, 44]. In the present example of coronene and HBC, however, we show unambiguously that also for systems with a quasi-two-dimensional periodicity, the band structure of the infinite counterpart, i.e. graphene, emerges from the molecular states of the finite quasi-periodic systems. By changing the size of the molecule, we can follow the evolution of the intramolecular electronic band dispersion, from coronene over HBC up to the infinite-sized graphene with the well-known Dirac point, which is absent in the graphene quantum wells of $\approx$1 nm size described here. Moreover, this approach offers the intriguing perspective of tuning the lateral intermolecular coupling by a (partial) substitution of the terminating hydrogen atoms.

6. Conclusion

We have demonstrated that the electronic structure of the polycyclic hydrocarbons coronene and HBC can be interpreted as lateral quantum dots of graphene. The molecules show discrete electronic energy levels that resemble the momentum dependence of the electronic band dispersion of graphene. The shape of the molecular orbitals of coronene or HBC leads to a characteristic angle dependence of the photoemission intensity, reflecting the spatial distribution of electrons in the graphene sheet. We have shown that the isolated planar molecule can be treated as a graphene quantum dot with distinct finite size effects. With basic textbook theory of cylindrical quantum wells, we can predict the position of the observed states of HBC in energy and momentum surprisingly well. Precise *ab initio* methods coincide with the quantum well states in energy and describe the complete ARPES signal very accurately. Therefore, the presented systems are basic model systems for more complex nanoscale graphene structures, such as ribbons or artificial quantum dots [45, 46].

Acknowledgments

This work was supported by the Deutsche Forschungsgemeinschaft (FOR 1162 and GRK 1221) and the Bundesministerium für Bildung und Forschung (contract numbers 05K10WW2 and 03SF0356B). PP acknowledges support from the Austrian Science Fund (FWF) under P23190-N16.

References

[1] Castro Neto A H, Guinea F, Peres N M R, Novoselov K S and Geim A K 2009 The electronic properties of graphene *Rev. Mod. Phys.* **81** 109–62
[2] Zhi L and Mullen K 2008 A bottom-up approach from molecular nanographenes to unconventional carbon materials *J. Mater. Chem.* **18** 1472–84
[3] Müllen K and Rabe J P 2008 Nanographenes as active components of single-molecule electronics and how a scanning tunneling microscope puts them to work *Accounts Chem. Res.* **41** 511–20
[4] Martínez-Blanco J, Klingsporn M and Horn K 2010 Selective adsorption of coronene on Si(1 1 1)-(7 × 7) *Surf. Sci.* **604** 523–8
[5] Fujihara M, Miyata Y, Kitaura R, Nishimura Y, Camacho C, Irle S, Iizumi Y, Okazaki T and Shinohara H 2012 Dimerization-initiated preferential formation of coronene-based graphene nanoribbons in carbon nanotubes *J. Phys. Chem.* C **116** 15141–5
[6] Seidel C, Ellerbrake R, Gross L and Fuchs H 2001 Structural transitions of perylene and coronene on silver and gold surfaces: a molecular-beam epitaxy liked study *Phys. Rev.* B **64** 195418
[7] Lackinger M, Griessl S, Heckl WM and Hietschold M 2002 Coronene on Ag(111) investigated by LEED and STM in UHV *J. Phys. Chem.* B **106** 4482–5
[8] Wagner C, Kasemann D, Golnik C, Forker R, Esslinger M, Müllen K and Fritz T 2010 Repulsion between molecules on a metal: monolayers and submonolayers of hexa-*peri*-hexabenzocoronene on Au(111) *Phys. Rev.* B **81** 035423
[9] Bürgi L, Petersen L, Brune H and Kern K 2000 Noble metal surface states: deviations from parabolic dispersion *Surf. Sci.* **447** L157–61
[10] Chiang T C 2000 Photoemission studies of quantum well states in thin films *Surf. Sci. Rep.* **39** 181–235
[11] Mugarza A and Ortega J E 2003 Electronic states at vicinal surfaces *J. Phys.: Condens. Matter* **15** S3281
[12] Mugarza A, Marini A, Strasser T, Schattke W, Rubio A, García de Abajo F J, Lobo J, Michel E G, Kuntze J and Ortega J E 2004 Accurate band mapping via photoemission from thin films *Phys. Rev.* B **69** 115422

[13] Hämäläinen S K, Sun Z, Boneschanscher M P, Uppstu A, Ijäs M, Harju A, Vanmaekelbergh D and Liljeroth P 2011 Quantum-confined electronic states in atomically well-defined graphene nanostructures *Phys. Rev. Lett.* **107** 236803

[14] Subramaniam D *et al* 2011 Wave function mapping in graphene quantum dots with soft confinement *Phys. Rev. Lett.* **108** 046801

[15] Phark S, Borme J, Vanegas A L, Corbetta M, Sander D and Kirschner J 2011 Direct observation of electron confinement in epitaxial graphene nanoislands *ACS Nano* **5** 8162–6

[16] Nicolay G, Reinert F, Schmidt S, Ehm D, Steiner P and Hüfner S 2000 Natural linewidth of the ag(111) l-gap surface state as determined by photoemission spectroscopy *Phys. Rev.* B **62** 1631–4

[17] Kilian L, Umbach E and Sokolowski M 2004 Molecular beam epitaxy of organic films investigated by high resolution low energy electron diffraction (SPA-LEED): 3,4,9,10-perylenetetracarboxylicacid-dianhydride (PTCDA) on ag(1 1 1) *Surf. Sci.* **573** 359–78

[18] Zou Y, Kilian L, Scholl A, Schmidt Th, Fink R and Umbach E 2006 Chemical bonding of PTCDA on Ag surfaces and the formation of interface states *Surf. Sci.* **600** 1240–51

[19] Ziroff J, Forster F, Schöll A, Puschnig P and Reinert F 2010 Hybridization of organic molecular orbitals with substrate states at interfaces: PTCDA on silver *Phys. Rev. Lett.* **104** 233004

[20] Kresse G and Furthmüller J 1996 Efficient iterative schemes for *ab initio* total-energy calculations using a plane-wave basis set *Phys. Rev.* B **54** 11169

[21] Blöchl P E 1994 Projector augmented-wave method *Phys. Rev.* B **50** 17953

[22] Perdew J P, Burke K and Ernzerhof M 1996 Generalized gradient approximation made simple *Phys. Rev. Lett.* **77** 3865

[23] Puschnig P, Berkebile S, Fleming A J, Koller G, Emtsev K, Seyller T, Riley J D, Ambrosch-Draxl C, Netzer F P and Ramsey M G 2009 Reconstruction of molecular orbital densities from photoemission data *Science* **326** 702–6

[24] Trevisanutto P E, Giorgetti C, Reining L, Ladisa M and Olevano V 2008 *Ab initio GW* many-body effects in graphene *Phys. Rev. Lett.* **101** 226405

[25] Berkebile S *et al* 2011 A momentum space view of the surface chemical bond *Phys. Chem. Chem. Phys.* **13** 3604–11

[26] Schwalb C H, Sachs S, Marks M, Scholl A, Reinert F, Umbach E and Hofer U 2008 Electron lifetime in a Sshockley-type metal–organic interface state *Phys. Rev. Lett.* **101** 146801

[27] Ziroff J, Gold P, Bendounan A, Forster F and Reinert F 2009 Adsorption energy and geometry of physisorbed organic molecules on Au(111) probed by surface-state photoemission *Surf. Sci.* **603** 354–8

[28] Marks M, Zaitsev N L, Schmidt B, Schwalb C H, Schöll A, Nechaev I A, Echenique P M, Chulkov E V and Höfer U 2011 Energy shift and wave function overlap of metal–organic interface states *Phys. Rev.* B **84** 081301

[29] Reinert F, Nicolay G, Schmidt S, Ehm D and Hüfner S 2001 Direct measurements of the l-gap surface states on the (111) face of noble metals by photoelectron spectroscopy *Phys. Rev.* B **63** 115415

[30] Koller G, Berkebile S, Oehzelt M, Puschnig P, Ambrosch-Draxl C, Netzer F P and Ramsey M G 2007 Intra- and intermolecular band dispersion in an organic crystal *Science* **317** 351–5

[31] Jung W S, Leem C S, Kim C, Park S R, Park S Y, Kim B J, Rotenberg E and Kim C 2010 Imaging the electron density in solids by using multi-Brillouin-zone angle resolved photoelectron spectroscopy *Phys. Rev.* B **82** 235105

[32] Berkebile S, Puschnig P, Koller G, Oehzelt M, Netzer F P, Ambrosch-Draxl C and Ramsey M G 2008 Electronic band structure of pentacene: an experimental and theoretical study *Phys. Rev.* B **77** 115312

[33] Berkebile S, Koller G, Puschnig P, Ambrosch-Draxl C, Netzer F P and Ramsey M G 2009 Angle-resolved photoemission of chain-like molecules: the electronic band structure of sexithiophene and sexiphenyl *Appl. Phys.* A **95** 101–5

[34] Puschnig P, Reinisch E-M, Ules T, Koller G, Soubatch S, Ostler M, Romaner L, Tautz F S, Ambrosch-Draxl C and Ramsey M G 2011 Orbital tomography: deconvoluting photoemission spectra of organic molecules *Phys. Rev.* B **84** 235427

[35] Seyller T, Bostwick A, Emtsev K V, Horn K, Ley L, McChesney J L, Ohta T, Riley J D, Rotenberg E and Speck F 2008 Epitaxial graphene: a new material *Phys. Status Solidi* b **245** 1436–46

[36] Paggel J J, Miller T, Luh D A and Chiang T C 2000 Quantum well photoemission from atomically uniform Ag films: determination of electronic band structure and quasi-particle lifetime in Ag(100) *Appl. Surf. Sci.* **162–163** 78–85

[37] Robinett R W 1996 Visualizing the solutions for the circular infinite well in quantum and classical mechanics *Am. J. Phys.* **64** 440–5

[38] Wu Y Z, Won C Y, Rotenberg E, Zhao H W, Toyoma F, Smith N V and Qiu Z Q 2002 Dispersion of quantum well states in Cu/Co/Cu(001) *Phys. Rev.* B **66** 245418

[39] Baumberger F, Hengsberger M, Muntwiler M, Shi M, Krempasky J, Patthey L, Osterwalder J and Greber T 2004 Localization of surface states in disordered step lattices *Phys. Rev. Lett.* **92** 196805

[40] Mugarza A, Schiller F, Kuntze J, Cordón J, Ruiz-Osés M and Ortega J E 2006 Modelling nanostructures with vicinal surfaces *J. Phys.: Condens. Matter* **18** S27

[41] Pennec Y, Auwaerter W, Schiffrin A, Weber-Bargioni A, Riemann A and Barth J V 2007 Supramolecular gratings for tuneable confinement of electrons on metal surfaces *Nature Nanotechnol.* **2** 99–103

[42] Jiutao Li, Wolf-Dieter Schneider, Richard Berndt and Crampin S 1998 Electron confinement to nanoscale Aag islands on Ag(111): a quantitative study *Phys. Rev. Lett.* **80** 3332–5

[43] Klappenberger F, Kühne D, Krenner W, Silanes I, Arnau A, García de Abajo F J, Klyatskaya S, Ruben M and Barth J V 2011 Tunable quantum dot arrays formed from self-assembled metal-organic networks *Phys. Rev. Lett.* **106** 026802

[44] Häming M, Ziroff J, Salomon E, Seitz O, Cahen D, Kahn A, Scholl A, Reinert F and Umbach E 2009 Electronic band structure and ensemble effect in monolayers of linear molecules investigated by photoelectron spectroscopy *Phys. Rev.* B **79** 155418

[45] Hengyi Xu, Heinzel T and Zozoulenko I V 2009 Edge disorder and localization regimes in bilayer graphene nanoribbons *Phys. Rev.* B **80** 045308

[46] Schelter J, Ostrovsky P M, Gornyi I V, Trauzettel B and Titov M 2011 Color-dependent conductance of graphene with adatoms *Phys. Rev. Lett.* **106** 166806